Atmos. Meas. Tech., 7, 2551–2566, 2014
www.atmos-meas-tech.net/7/2551/2014/
doi:10.5194/amt-7-2551-2014

Atmospheric Measurement Techniques
Open Access

Development of a cavity-enhanced aerosol albedometer

W. Zhao[1,2], X. Xu[1,2], M. Dong[1,2], W. Chen[3], X. Gu[1,2], C. Hu[1,2], Y. Huang[1], X. Gao[1,2], W. Huang[1,2], and W. Zhang[1,2]

[1]Key Laboratory of Atmospheric Composition and Optical Radiation, Anhui Institute of Optics and Fine Mechanics, Chinese Academy of Sciences, Hefei 230031, Anhui, China
[2]Laboratory of Atmospheric Physico-Chemistry, Anhui Institute of Optics and Fine Mechanics, Chinese Academy of Sciences, Hefei 230031, Anhui, China
[3]Laboratory of Physico-Chemistry of the Atmosphere, University of the Littoral Opal Coast, 59140 Dunkerque, France

Correspondence to: W. Zhang (wjzhang@aiofm.ac.cn)

Received: 11 February 2014 – Published in Atmos. Meas. Tech. Discuss.: 26 March 2014
Revised: 2 July 2014 – Accepted: 2 July 2014 – Published: 18 August 2014

Abstract. We report on the development of a cavity-enhanced aerosol single-scattering albedometer based on incoherent broadband cavity-enhanced absorption spectroscopy (IBBCEAS) combined with an integrating sphere (IS) for simultaneous in situ measurements of aerosol scattering and extinction coefficients in an exact same sample volume. The cavity-enhanced albedometer employed a blue light-emitting-diode (LED)-based IBBCEAS approach for the measurement of wavelength-resolved aerosol optical extinction over the spectral range of 445–480 nm and an integrating sphere nephelometer coupled to the IBBCEAS setup for the measurement of aerosol scattering. The scattering signal was measured with a single-channel photomultiplier tube (PMT), providing an averaged value over a narrow bandwidth (full-width at half-maximum, FWHM, ∼ 9 nm) in the spectral region of 465–474 nm. A scattering coefficient at a wavelength of 470 nm was deduced as an averaged scattering value over the spectral region of 465–474 nm and used for data analysis and instrumental performance comparison. Performance evaluation of the albedometer was carried out using laboratory-generated particles and ambient aerosol. The scattering and extinction measurements of monodisperse polystyrene latex (PSL) spheres generated in the laboratory proved excellent correlation between two channels of the albedometer. The retrieved refractive index (RI) of the PSL particles from the measured scattering and extinction efficiencies agreed well with the values reported in previously published papers. Aerosol light scattering and extinction coefficients, single-scattering albedo (SSA) and NO_2 concentrations in an ambient sample were directly and simultaneously measured using the albedometer developed. The instrument developed was validated via an intercomparison of the measured aerosol scattering coefficients and NO_2 trace gas concentrations to a TSI 3563 integrating nephelometer and a chemiluminescence detector, respectively.

1 Introduction

Atmospheric aerosols influence climate by modifying the Earth's energy balance through absorption and scattering of the incoming solar radiation (direct effects), changing the cloud properties and abundance (indirect effects), as well as the thermal structure of the atmosphere and the surface energy budget (semi-direct effects) (Ghan and Schwartz, 2007; Stier et al., 2007).

This radiative forcing (RF) capacity, characterized by the aerosol single-scattering albedo (SSA, ω) and its complex refractive index (RI), is mainly determined by the aerosol optical properties (scattering, absorption and extinction). The evaluation of the aerosol impact on climate thus requires accurate, widespread and unbiased quantification of its optical properties as a function of the solar radiation wavelength, of their chemical composition and size distribution (Boucher et al., 2013).

Development of appropriate and well-adapted measurement technologies for real-time in situ measurement of aerosol optical properties is an important step towards a more accurate and quantitative understanding of the aerosol climate effect (Strawa et al., 2003; Thompson et al., 2008).

Aerosol single-scattering albedo, defined as the ratio of the aerosol scattering (α_{scat}) to its total extinction (α_{ext})

coefficient, governs the relative strength of the aerosol scattering and absorption capacity. The value of SSA ranges from 0 for a completely absorbing particle to 1 for a purely scattering particle (Ramanathan et al., 2001; Chin et al., 2009; Hallquist et al., 2009). The in situ accurate measurement of SSA is a key challenge in atmospheric science and climate change research (Moosmüller et al., 2009; Yu et al., 2012; Petzold et al., 2013).

Since the aerosol extinction coefficient is the sum of the absorption and scattering coefficients, a commonly used method for the determination of SSA is to separately measure two of the three optical parameters – absorption, scattering and extinction coefficients – with different instruments. In general, the aerosol absorption coefficient is measured with filter-based techniques or the photoacoustic spectroscopy (PAS) technique (Sheridan et al., 2005; Slowik et al., 2007; Cross et al., 2010; Lack et al., 2014). The scattering coefficient is usually measured with an integrating nephelometer and the extinction coefficient can be measured with an optical extinction cell or cavity-enhanced/ring-down spectroscopy (Moosmüller et al., 2009). Improving the detection sensitivity and the measurement accuracy for each optical parameter is of the first importance to improve the measurement accuracy of SSA.

Filter-based instruments, such as particle soot absorption photometers (PSAP), aethalometer and multi-angle absorption photometers (MAAP), are simple, low-cost and insensitive to gaseous absorption. These techniques suffer, however, from the fact that the natural suspended state of the aerosol changed after deposition (Subramanian et al., 2007). The measurements are strongly influenced by the filter type, multiple scattering by the filter medium and the angular distribution of the scattered light (Moosmüller et al., 2009). The measurement uncertainties of the filter-based techniques are typically between 20 and 30 % for laboratory-generated, dry, non-absorbing or strongly absorbing particles (Bond et al., 1999). For high relative humidity (RH) or high light-absorbing organic aerosol loadings, the bias in filter-based light absorption measurement may be larger than 100 %. With real-time correction for scattering artifacts, the MAAP instrument can achieve a measurement uncertainty of ~ 12 % for pure soot (Cappa et al., 2008; Lack et al., 2008).

The PAS method provides excellent detection sensitivity and time response (0.08 Mm^{-1}, with 60 s average) for direct in situ measurement of aerosol light absorption. The reported accuracy ranges from 5 to 10 % (Lack et al., 2006; Arnott et al., 2003). Recently, Langridge et al. (2013) reported a laboratory study on aerosol absorption measurement using PAS at high RH. They concluded that the PAS is not a technique well suited to the measurement of aerosol absorption at high RH due to the impact of water evaporation on PAS signal. The recommended RH in PAS measurements should be controlled in the range of 10–30 %.

Regarding scattering measurements with nephelometers, an important limitation is represented by the measurement truncation angles: light scattered at angles smaller and larger than the truncation angles can not be detected. For instance, for TSI 3563 integrating nephelometer, measurements of scattering light are limited to between 7 and 170°. The truncation errors lead to the underestimation of scattering coefficients, particularly for particles with large size. The uncertainty in scattering measurements using a nephelometer varies from 5 to 50 % depending on the particle size and the relative humidity (Massoli et al., 2009). Theoretical calculations suggest higher truncation errors for absorbing aerosols due to changes in the scattering phase function (Moosmüller and Arnott, 2003). Correction factors for the truncation errors can be calculated using Mie theory based on the knowledge of the measured Ångström exponent, aerosol size distribution and the complex refractive index (RI, $m = n + ik$, where n and k correspond to the real and imaginary part of the RI, respectively) (Anderson and Ogren, 1998; Massoli et al., 2009; Müller et al., 2009). A nearly ideal integrating nephelometer was developed by Varma et al. (2003). The reported nephelometer used an integrating sphere (IS) coupled to two truncation reduction tubes to integrate the scattered light. The forward (backward) truncation angles were reduced to $\sim 1°$ ($\sim 179°$).

Measurements of optical extinction using single pass cells are limited by the detection sensitivity and are of practical use only for laboratory-generated aerosols or near-source aerosol plumes in the ambient atmosphere (Schnaiter et al., 2003; Virkkula et al., 2005; Chartier and Greenslade, 2012). Cavity-enhanced/ring-down spectroscopy provides highly sensitive and accurate methods for α_{ext} measurement. The detection sensitivity can be better than 1 Mm^{-1} with an accuracy of < 3 % (Sappey et al., 1998; Smith and Atkinson, 2001; Thompson et al., 2002; Brown, 2003; Pettersson et al., 2004; Moosmüller et al., 2005; Kebabian et al., 2007; Abo Riziq et al., 2007; Zhang et al., 2008; Lang-Yona et al., 2009; Massoli et al., 2010; Li et al., 2011; Mellon et al., 2011; Bluvshtein et al., 2012; Michel Flores et al., 2012; Wang et al., 2012).

Separate measurement of the extinction coefficient with the cavity-enhanced/ring-down method and of the absorption coefficient with the photoacoustic technique has been used for highly sensitive measurement of aerosol single-scattering albedo without changing the dispersed state of the aerosol particles (Langridge et al., 2011; Lack et al., 2012). However, as this still involves different instruments for separate measurements of extinction and absorption coefficients under different sampling conditions, it might cause potential errors in the determination of the SSA value because the aerosol optical properties are very sensitive to the sampling conditions such as temperature and RH (Lack et al., 2008).

Various spectroscopic approaches have been developed for simultaneous measurement on an exact same sample volume to overcome this weakness, such as the integrated photoacoustic nephelometer (Abu-Rahmah et al., 2006; Chakrabarty et al., 2007, 2010; Lewis et al., 2008; Sharma et al., 2013) and the cavity ring-down nephelometer

(Strawa et al., 2003, 2006; Sanford et al., 2008). An aerosol albedometer incorporating a ring-down cavity and an integrating sphere for simultaneous measurement of optical scattering and extinction at a fixed frequency was developed by Thompson et al. (2008) (Dial et al., 2010; Ma and Thompson, 2012; Wei et al., 2013a, b; Ma et al., 2013). The relative measurement uncertainty in SSA achieved by this device, dependent upon the particle loading, is better than 5 % (with detection sensitivities of 2.7 Mm^{-1} and 0.6 Mm^{-1} for scattering and extinction, respectively), which holds promise for sensitive measurement of SSA.

In this paper, we report on the development of a cavity-enhanced aerosol single-scattering albedometer based on incoherent broadband cavity-enhanced absorption spectroscopy (IBBCEAS) incorporating an integrating sphere (IS) for direct in situ measurement of aerosol scattering and extinction coefficients in the exact same sample volume. Truncation reduction tubes were used to minimize the truncation angle (reduced to be within $\sim 1.2°$ for the forward (backward) truncation angle) as reported by Varma et al. (2003). The cavity-enhanced albedometer employed the IBBCEAS method for the measurement of the aerosol extinction spectrum over the spectral range of 445–480 nm and the scattering signal was measured in an IS associated with a single-channel PMT (photomultiplier tube), providing an integrated result over a narrow bandwidth of ~ 9 nm (full-width at half-maximum, FWHM) in the spectral region of 465–474 nm. A scattering coefficient at a wavelength of 470 nm was deduced as an averaged scattering value over the effective bandwidth and used for data analysis and instrumental-performance comparison. Evaluation of the albedometer was carried out using laboratory-generated particles and ambient aerosol for both scattering and extinction channels.

IBBCEAS, first proposed by Fiedler et al. (2003), combining a broadband light source with a high-finesse optical cavity, has recently been used for broadband-wavelength-resolved aerosol extinction measurements (Thompson and Spangler, 2006; Ball et al., 2004; Varma et al., 2009, 2013; Thalman and Volkamer, 2010; Wilson et al., 2013; Zhao et al., 2013; Washenfelder et al., 2013). The main advantage of broadband measurement over single-wavelength measurement is its capacity to simultaneously measure multiple species present in air sample (gases and aerosol) using a single instrument. A DOAS (differential optical absorption spectroscopy)-type data processing approach (spectral-fitting algorithm) is applied to address the spectral-interference issue and selectively retrieve gas concentrations from non-structured aerosol extinction features (Berden and Engeln, 2009; Fayt et al., 2011; Gherman et al., 2008; Kraus and Geyer, 2001; Platt et al., 2009; Platt and Stutz, 2008; Thalman and Volkamer, 2010; Zhao et al., 2013).

In the present work, measurement intercomparisons of the cavity-enhanced albedometer developed were carried out using a Thermo 42i NO_x analyzer (equipped with a molybdenum converter) for NO_2 trace concentration measurement and a TSI 3563 nephelometer for aerosol scattering coefficient measurement. The good agreement observed in these instrumental intercomparisons demonstrated that the albedometer developed provided a robust method for direct and simultaneous measurement of aerosol scattering and extinction coefficients (and then SSA) and the concentrations of absorbing gas present in the air sample.

2 Experimental setup

The scheme of the cavity-enhanced albedometer developed in the present work is shown in Fig. 1. The broadband radiation was provided by a blue LED (LedEngin LZ110B200) with an emission spectrum peaked at 465 nm. The LED was mounted on a peltier heat sink to stabilize the emission intensity. Light was coupled directly from the LED into a multimode fiber of 500 µm core diameter with a numerical aperture (NA) of 0.22 (Ocean Optics). The emerging light from the fiber was focused with a 75 mm focal-length achromatic plano-convex lens to the center of a high-finesse optical cavity. A bandpass filter, centered at 450 nm with an FWHM of 40 nm (Thorlabs FB 450-40), was located in front of the cavity. The optical cavity consisted of an integrating sphere and two truncation reduction tubes (200 mm long, with an inner diameter of 18 mm). The beam diameter in the cavity was about 12 mm. Using a well-collimated beam was helpful in reducing the wall scattering effects. High-reflectivity mirrors (LGR, 0.8 in. in diameter and 6 m radius of curvature, $R > 99.99$ % between 415 and 465 nm) were mounted on each end of the truncation reduction tubes. The distance between two mirrors (d) was 600 mm. Each mirror was isolated from the air sample flow by a purge volume that was continuously flushed with dry zero air at a rate of 0.09 L min^{-1} to prevent degradation of the mirror reflectivity by aerosol deposition. The distance L from sample inlet to the outlet was about 470 mm. The continuous air sample flow rate through the cavity cell was 1.5 L min^{-1} at atmospheric pressure (~ 99 kPa, monitored with a pressure gauge). With this flow rate, the residence time was about 200 s for the present albedometer (with a total volume of ~ 1.9 L including the truncation reduction tubes). Light transmitted through the cavity was collected with a 50 mm focal length achromatic lens and coupled into a multi-mode optical fiber of 500 µm core diameter and 0.22 NA. The output of the fiber was directly connected to a spectrometer (Ocean Optics QE65000) equipped with a 100 µm wide slit resulting in a spectral resolution of 0.4 nm over the wavelength range of 412–487 nm (measured using a low-pressure mercury lamp emission). Temperature and relative humidity were measured with a hygrometer (Rotronic, model HC2 humidity sensor).

The integrating sphere, machined from solid aluminum, was segmented into two hemispheres with an inner diameter d_0 of 150 mm. Its inside layer consisted of pressed PTFE (with a uniform reflectivity of > 99 % between 200

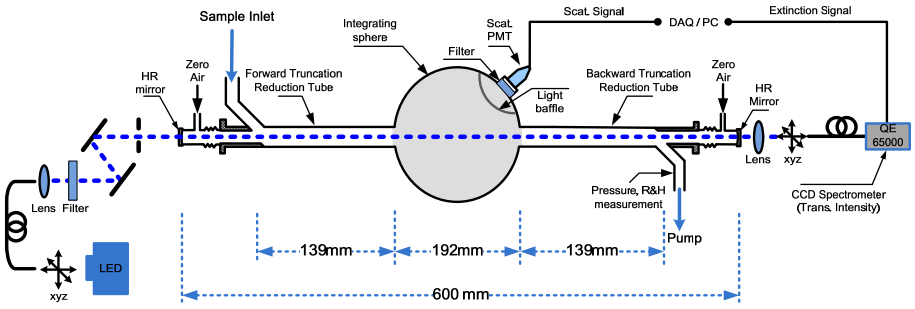

Figure 1. Schematic diagram of the blue LED-based cavity-enhanced albedometer developed.

and 2500 nm). The internal volume of the sphere was about 1.8 L. A 16 mm diameter hole was present at each pole of the hemisphere for the passage of the probe light beam. A third hole of identical size, located on the side wall of one hemisphere, was used for scattering signal measurement using a photomultiplier tube (PMT, ZOLIX PMTH-S1-CR131A). A 20 mm wide light baffle, made of PTFE, was used to prevent light scattered by the medium from directly reaching the PMT. A bandpass filter, which centered at 470 nm with an FWHM of ~ 9 nm ($470\,\mathrm{nm}^{+4}_{-5}$), was located in front of the PMT to eliminate the ambient stray light. The PMT signal was acquired with a data acquisition (DAQ) card (National Instruments, NI PCIe-6351), which provided an integrated scattering signal over the spectral region of 465–474 nm.

3 Results and discussion

3.1 Angular nonidealities of the albedometer

The forward-scattering truncation geometry of the cavity-enhanced albedometer developed and a plot of truncation angles as a function of the distance d_e from the scattering location in the sphere to the exit or entrance aperture are shown in Fig. 2. Following Varma et al.'s (2003) discussion, the forward-scattering truncation angle of our albedometer varied from 3.1 to 90° with an average of 12.2° for the integrating sphere without truncation reduction tube. The effective truncation angle $\alpha(d_e) = \tan^{-1}[r/(d_e + d_0)]$ varied from 1.2 to 3.1° (d_e and d_0 are schematized in the figure and $r = 8$ mm, the radius of the hole presented at each pole of the hemisphere for the passage of the probe light beam.), with an average value of 1.8° for particles located in the truncation reduction tube at a distance d_e from the entrance aperture.

Figure 3 shows the size-dependent truncated fraction of total scattering for various truncation angles (Baynard et al., 2007). Four different truncation angles were used in the calculations with different d_e, representing different geometries: (1) 0–1.22°, with $d_e = (d - d_0)/2$, where d is the distance between two cavity mirrors; (2) 0–1.48°, $d_e = (L - d_0)/2$, with L the distance from the sample inlet to the outlet; (3) 0–3.1°, for the integrating sphere without truncation reduction

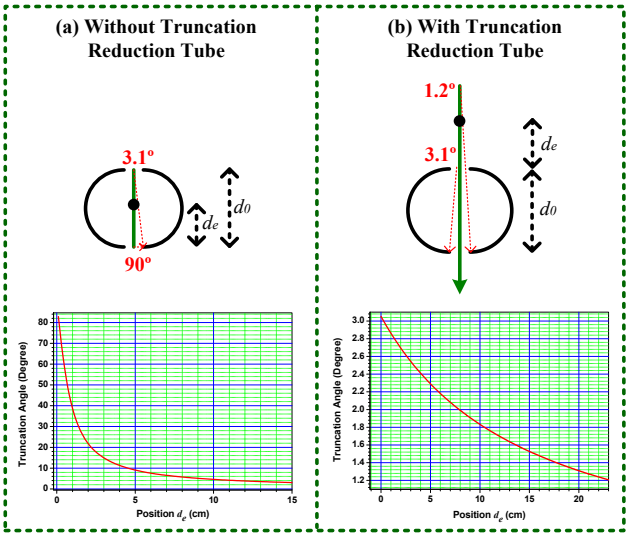

Figure 2. Forward-scattering truncation geometry of the cavity-enhanced albedometer and plot of truncation angles as a function of the distance d_e from the scattering location in the sphere (marked with a black dot) to the exit or entrance aperture: **(a)** without and **(b)** with truncation reduction tube.

tubes and (4) 0–7°, in the case of TSI 3563 nephelometer (as specified by the manufacturer). The truncated fraction of total scattering was calculated with Mie scattering theory for spherical monodisperse particles with an RI of $m = 1.6 + i0$ at $\lambda = 470$ nm. For 1 µm diameter particle, truncated fractions of total scattering were 0.22 % and 1.4 % with (truncation angle of 1.22°) and without (truncation angle of 3.1°) truncation reduction tubes, respectively. The truncation reduction tubes compensated for the near-forward-scattered intensity, and reduced the measurement errors in large-particle scattering measurements. This value of 0.22 % was much smaller than the value of 6.4 % from the TSI nephelometer. The small truncation angle (0–1.22°) of our IS system significantly reduced truncation errors for large particles when compared with a TSI nephelometer.

3.2 Data retrieval processing

In the IBBCEAS approach, wavelength-resolved aerosol extinction can be calculated using the following equation (Fiedler et al., 2003; Washenfelder et al., 2008, 2013):

$$\begin{aligned}\alpha_{\text{Total Ext}}(\lambda) &= \alpha_{\text{Aerosol Ext}}(\lambda) + \alpha_{\text{Gas Abs}}(\lambda) + \alpha_{\text{Gas Rayleigh}}(\lambda) \\ &= R_{\text{L}}\left(\frac{(1-R(\lambda))}{d} + \alpha_{\text{Gas Rayleigh}}(\lambda)\right) \\ &\cdot\left(\frac{I_0(\lambda)-I(\lambda)}{I(\lambda)}\right), \end{aligned} \quad (1)$$

where three components included in the measured total extinction $\alpha_{\text{Total Ext}}(\lambda)$ – $\alpha_{\text{Aerosol Ext}}(\lambda)$, $\alpha_{\text{Gas Abs}}(\lambda)$ and $\alpha_{\text{Gas Rayleigh}}(\lambda)$ – correspond to the aerosol extinction, gas phase absorption and Rayleigh scattering by the gas, respectively. R_{L} is the ratio of the total cavity cell length (d, the distance between two mirrors) to the real cell length containing the air sample when the cavity mirror is purged with gas flow. R_{L} can be determined using an absorber with known extinction (such as a dilute concentration of NO_2) or geometrically measured based on the assumption that aerosols follow the gas flow path and are not present in the purging volumes (Washenfelder et al., 2013). In this work, R_{L} was determined from the absorption measurement of 42 ppbv NO_2 with and without mirror purging. $R(\lambda)$ is the mirror reflectivity; d is the distance between two cavity mirrors; $I_0(\lambda)$ and $I(\lambda)$ are the light intensities transmitted through the cavity without and with air samples, respectively. In our experiment, both the $I_0(\lambda)$ and $I(\lambda)$ spectra were more conveniently obtained in N_2 or air; the gas Rayleigh scattering was presented in both spectra and hence canceled. The measured extinction can be rewritten as follows (Washenfelder et al., 2013):

$$\begin{aligned}\alpha_{\text{Ext,Meas}}(\lambda) &= \alpha_{\text{Aerosol Ext}}(\lambda) + \alpha_{\text{Gas Abs}}(\lambda) \\ &= R_{\text{L}}\frac{(1-R(\lambda))}{d}\left(\frac{I_0(\lambda)-I(\lambda)}{I(\lambda)}\right). \end{aligned} \quad (2)$$

Broadband extinction measurement with IBBCEAS provides a robust method for simultaneous and selectively quantitative measurement of both aerosol extinction and absorbing trace gases concentrations using a single instrument. The gas phase absorption can be extracted from the total extinction using the following equation:

$$\alpha_{\text{Ext,Meas}}(\lambda) = \sum n_i\sigma_i(s_i + t_i\lambda) + P(\lambda). \quad (3)$$

The first term describes the contribution from multiple gas absorptions and the second includes the contribution from wavelength-dependent aerosol extinction. Where n_i and σ_i are the number density and the absolute absorption cross section of the ith absorber, respectively, s_i and t_i are the shift and stretch coefficients for each absorber, used to reconstruct an accurate wavelength calibration. The polynomial offset $P(\lambda)$, varying from linear to fifth order, is used to account for the variation in spectral background, including wavelength-dependent aerosol extinction and spectral-baseline shift (which can be considered as system drift in the extinction measurement). In the present work, a third-order polynomial function was used for data retrieval. For a particle-free sample, $P(\lambda)$ merely represents the spectral-baseline drift including baseline variation due to Rayleigh scattering by air and unspecified background change in spectra resulting from unstable LED emission and/or unstable dark current variation in the CCD (charge coupled device) spectrometer. For this reason, high stability of an IBBCEAS instrument is highly required for high-accuracy measurements of aerosol extinction such that the background drift could be negligible in comparison with the measured aerosol extinction.

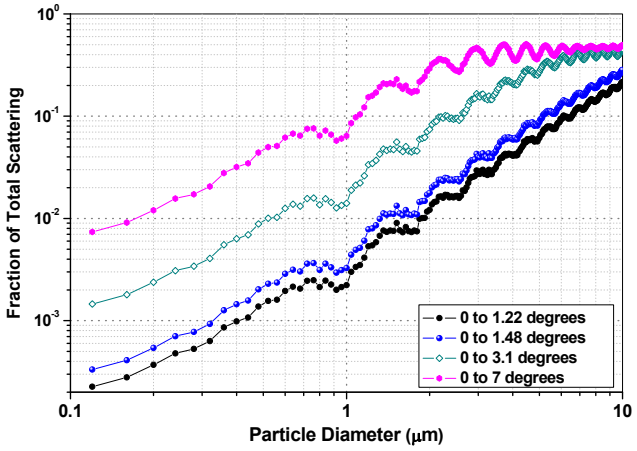

Figure 3. Size dependence of the truncated fraction of total scattering under different truncation angles: (1) 0–1.22°, calculated with $d_{\text{e}} = (d - d_0)/2$; (2) 0–1.48°, with $d_{\text{e}} = (L - d_0)/2$; (3) 0–3.1°, without truncation reduced tubes, and (4) 0–7° for the TSI Nephelometer used. The simulations were made based on Mie scattering theory applied to monodisperse particles with a refractive index of $m = 1.6 + i0$ at $\lambda = 470$ nm.

Mirror reflectivity $R(\lambda)$ of the albedometer was determined by introducing gases with different Rayleigh cross sections (Moosmüller et al., 2005; Washenfelder et al., 2008; Zhao et al., 2013; Dong et al., 2013). In this work, the $R(\lambda)$ was determined from the difference in the transmitted intensities of N_2 and SF_6. The cavity was flushed with N_2 and SF_6 at 1.5 L min^{-1} rate for 40 min for each species, until the transmitted light intensity attained a stable value. The Rayleigh cross sections used for the mirror reflectivity calculation were reported by Naus and Ubachs (2000) and Sneep and Ubachs (2005), with an experimental uncertainty in cross section of 1 % for N_2 and 3 % for SF_6. The mirror reflectivity was found to be about 99.96 % at 470 nm. During the process of mirror reflectivity calibration, the purging zero-air flow was turned off and the cavity was fully filled with

calibration gases. For aerosol measurement, the purging zero air was continuously used, which shortened the effective path length.

The aerosol scattering coefficient, α_{scat}, is proportional to the ratio of the scattering signal (I_{scat}) measured with a PMT and the transmitted intensity (I_{trans}) measured with a CCD spectrometer (the same spectrometer used for the IBBCEAS measurement) (Strawa et al., 2003; Thompson et al., 2008):

$$\alpha_{\text{scat}} = \frac{I_{\text{scat}}}{I_{\text{trans}}} \frac{(1-R)}{(1+R)\,d} K = \frac{I_{\text{scat}}}{I_{\text{trans}}} K', \quad (4)$$

where K and K' are the experimentally determined calibration constants that account for the differences in collection efficiency and response of different type of detectors, respectively. When purging gas was continuously introduced into the albedometer, the effective path length and thus the reduction tube length was shortened. However, for particle diameters smaller than 2 µm, the truncation error was smaller than 2 %, and therefore the purging gas effect (R_{L} factor) might be neglected for the scattering measurement of our albedometer. The calibration of the parameter K' can be made based on the assumption of a linear response of the PMT to the scattering light intensity (Anderson et al., 1996). K' might be simply calibrated with CO_2 and N_2 scattering processes by the following equation:

$$K' = \left(\alpha_{\text{scat\_CO}_2} - \alpha_{\text{scat\_N}_2}\right) \Big/ \left(\frac{I_{\text{scat\_CO}_2}}{I_{\text{trans\_CO}_2}} - \frac{I_{\text{scat\_N}_2}}{I_{\text{trans\_}N_2}} \right), \quad (5)$$

where $\alpha_{\text{scat\_CO}_2}$ and $\alpha_{\text{scat\_N}_2}$ are the theoretically calculated Rayleigh scattering coefficients of CO_2 and N_2. $I_{\text{scat\_CO}_2}$ and $I_{\text{scat\_N}_2}$ are experimentally measured scattering intensities when the cavity is filled with CO_2 or N_2, respectively. $I_{\text{trans\_CO}_2}$ and $I_{\text{trans\_N}_2}$ are the measured transmitted intensity of the cavity (at $\lambda = 470$ nm in our case) for CO_2 and N_2, respectively.

In order to calibrate the scale factor K' well, He and SF_6 were used to extend the dynamical range (from 0.3 to 145 Mm^{-1}) of the calibration. The Rayleigh scattering cross section for He was fitted to Shardanand and Rao's data ($\sigma_{\text{Rayleigh He}} = 1.336 \times 10^{-17} \times \lambda^{-4.1287}$) (Shardanand and Rao, 1977; Washenfelder et al., 2013). The cross sections of N_2, CO_2 and SF_6 were obtained from Naus and Ubachs (2000) and Sneep and Ubachs (2005). Calibration of K' was achieved by flushing the cavity with calibration gases and then performing measurements of the I_{scat} / I_{trans} ratio. A linear fit of the theoretical Rayleigh scattering coefficient of each gas to the measured I_{scat} / I_{trans} ratio is shown in Fig. 4a. As can be seen, the measured I_{scat} / I_{trans} signal is linearly correlated with the theoretically calculated Rayleigh scattering coefficient. The intercept of the I_{scat} / I_{trans} ratio was considered as the contribution of the photon counts due to scattering by internal surfaces.

A regression plot of the measured extinction and scattering coefficients for calibration gases is shown in Fig. 4b,

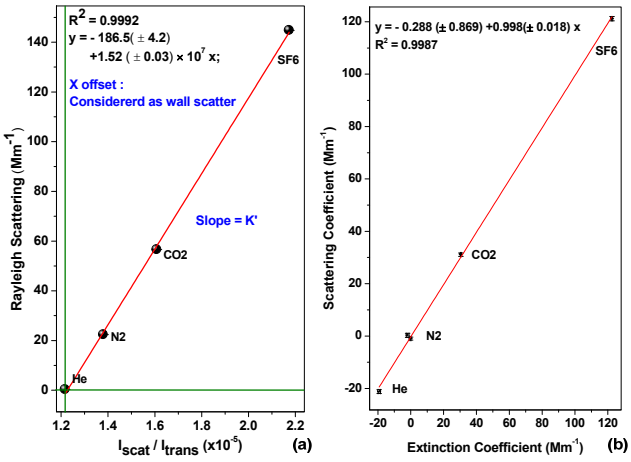

Figure 4. Calibration of the scaling factor K' of the cavity-enhanced albedometer for the scattering channel with He, N_2, CO_2 and SF_6 at $\lambda = 470$ nm. **(a)** Plot of $I_{\text{scat}}/I_{\text{tans}}$ ratio vs. theoretical value of the Rayleigh scattering coefficient of each gas. **(b)** Regression plot of the measured extinction and scattering coefficients for calibration.

which proves an excellent correlation between the scattering and the extinction measurements (scattering = -0.288 (± 0.869) + 0.998 (± 0.018) × extinction, with $R^2 = 0.9987$).

3.3 Precision and accuracy of the instrument

The detection limits for the measurement of the scattering and extinction coefficients at 470 nm were determined by an Allan variance analysis. Figure 5 shows an Allan deviation plot realized based on 5.5 h time series measurements of a particle-free zero-air sample with a time resolution of 9 s. Longer-term drift of the instrument was observed which was smaller than 2 Mm^{-1} (as shown in the upper panel of Fig. 5). The scattering measurement channel exhibited the lowest detection limit of 0.07 Mm^{-1}, with an optimum integration time of 459 s that was much longer than the optimum integration time for the extinction measurement channel (54 s). With 54 s integration time, the detection limits for the scattering and extinction channels were 0.22 Mm^{-1} and 0.09 Mm^{-1}, respectively.

In the lower panel of Fig. 5, frequency distributions of the scattering and extinction measurements are shown. A Gaussian distribution was fitted to the histograms to obtain the mean of the zero-air measurements and the standard deviation (Kennedy et al., 2011; Dorn et al., 2013). The 1σ standard deviation of the Gaussian fit is a measure of the instrument measurement precision. The determined extinction measurement precision of 0.51 Mm^{-1} (in 9 s) is comparable to the result of 0.19 Mm^{-1} (with 10 s average time) reported by Petzold et al. (2013).

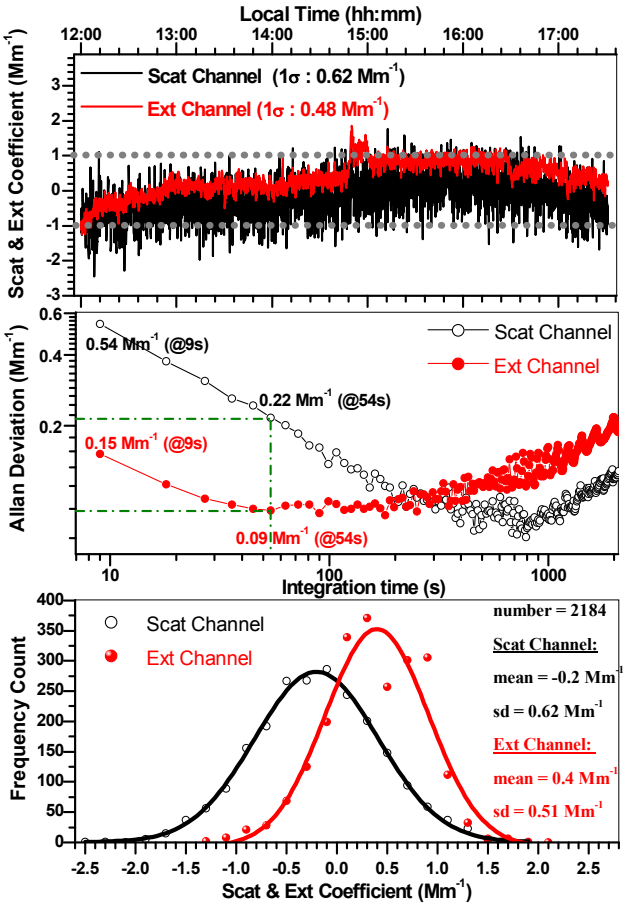

Figure 5. Time series of a 5.5 h measurement of a particle-free zero-air sample with a time resolution of 9 s (upper panel) and corresponding Allan deviation plots (middle panel) for both the scattering and extinction channels. The lower panel shows frequency distributions of the performed scattering and extinction measurements. A normal distribution was fitted to the histograms. The 1σ standard deviation, SD, is a measure of the instrument precision; "mean" denotes the mean scattering or extinction coefficients.

For aerosol measurement, the accuracy in the extinction measurement is mainly limited by the uncertainties in $(1-R)$, R_L and particle losses in the cavity. The drift of the LED intensity is not included when considering the accuracy of the extinction measurements, since frequent recording of I_0 (for example, every hour) could allow correction for the baseline drift related to the fluctuation in LED emission intensity. The cavity was flushed with N_2 and SF_6 at a rate of 1.5 L min^{-1} for 40 min for each species, until the transmitted light intensity attained a stable value. Ten different pairs of N_2 and SF_6 transmission spectra under stable conditions were used for mirror reflectivity determination, and then 10 values of the mirror reflectivity were averaged. The mean value used as mean mirror reflectivity and the mean relative error of $(1-R)$ is less than 1 %. We estimated an uncertainty of 3 % in R_L. The particle loss through the system, determined via the measurements from two condensation particle counters installed at the inlet and the outlet, respectively, was estimated to be 2 %. Considering all of the uncertainties, the total uncertainty in the extinction measurement was estimated to be less than 5 %.

The uncertainty in the scattering measurement is mainly caused by the uncertainties in K', the error caused by the angular nonidealities (less than 2 % for particle diameter smaller than 2 µm) and particle loss in the cavity. The uncertainty of K' was less than 2 %. The total uncertainty in scattering measurement was estimated to be about 4 %.

The total uncertainty in the measurement of SSA was then estimated to be less than 5 %, where the $(1-R)$ and R_L errors were considered as the total extinction error, while the errors in K', and the angular nonidealities were considered as the total scattering error. Since the scattering and extinction coefficients were measured on the exact same volume, the uncertainty of SSA for monodispersed aerosol due to particle loss could be ignored. However, for particle diameters larger than 2 µm, the influence of truncation errors for the finite acceptance angle measurements may be potential error sources.

3.4 Instrument test using laboratory-generated particles

Performance evaluation of the albedometer developed was performed with the measurements of laboratory-generated, monodispersed polystyrene latex (PSL) spheres. The aerosol generation system was the same as used in our previous work (Zhao et al., 2013). Aerosols were generated with a constant output atomizer (TSI-3076). PSL standards of four different diameters (200, 240, 300 and 400 nm) were generated by an electrostatic classifier (TSI differential mobility analyzer, DMA 3080 L) for the evaluation. The particle concentration was determined with two condensation particle counters (a CPC 3775 at the entrance of the cavity and a CPC 3776 at the exit of the cavity). After taking into account the dilution inside the cavity as a result of the purge flow of zero air on the mirrors, the averaged particle number was used for data analysis.

Laboratory-generated NaCl particles were used for the evaluation of particle loss vs. their size (as shown in Fig. 6). The particle loss is determined by the difference in particle concentrations measured by the two CPCs. For particle diameters larger than 300 nm, the particle loss can be ignored.

The time response of the instrument is evaluated using laboratory-generated, monodispersed PSL particles with a diameter of 240 nm. Figure 7 shows the time responses for the measurements of the particle concentration inside the integrating sphere and the measurements of the corresponding scattering and extinction coefficients using the cavity-enhanced albedometer. The rise time (from zero to its final stable value) for measurements of particle concentrations varying from 0 to 393 particle cm^{-3} was about 190 s, and the

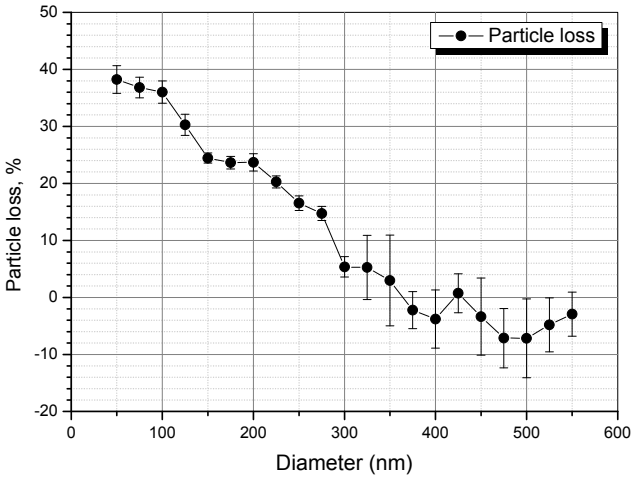

Figure 6. Laboratory assessment of the particle loss vs. particle size in the albedometer developed.

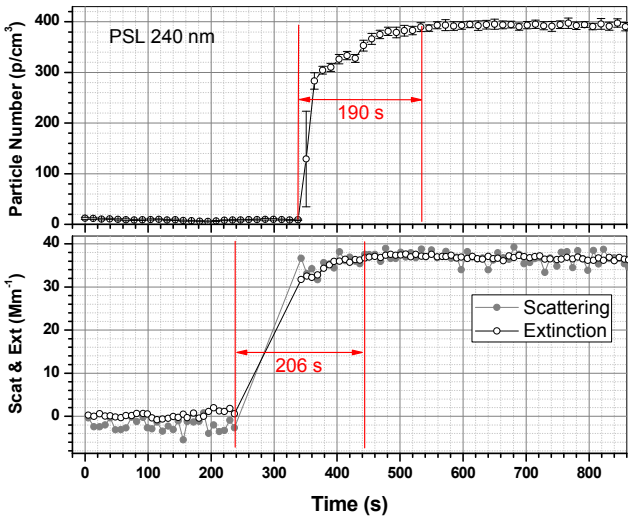

Figure 7. Time response of the cavity-enhanced albedometer developed to a variety of particle numbers from 0 to 393 particle cm^{-3} (corresponding to scattering and extinction coefficients of 37 Mm^{-1}, evaluated with monodispersed PSL particles with a diameter of 240 nm). Upper panel: rise time for the measurements of particle number concentration inside the albedometer with a TSI CPC 3776. Lower panel: the time response for the scattering and extinction coefficient measurements.

rise time for the measurements of the corresponding scattering and extinction coefficients (37 Mm^{-1}) was about 206 s.

Figure 8a shows a regression plot of the extinction (α_{ext}) and scattering (α_{scat}) coefficients at $\lambda = 470$ nm. The scattering and extinction data were averaged over 5 to 10 min sequences after the aerosol number concentration in the albedometer was sufficiently stable. Error bars in the figure correspond to 1σ of the sequence average. For the measurements of different PSL number concentrations or diameters, the cavity was washed with zero air for acquisition of the $I_0(\lambda)$ spectrum in order to correct for drifts in the background spectrum. The transmitted and scattered intensities of the particle-free air sample were used to subtract the light scattered by internal surfaces and by gas portions of the sample. The non-absorbing PSL sphere experiments had excellent correlation between the scattering and extinction measurements from the albedometer.

A plot of the experimentally measured scattering and extinction coefficients vs. the averaged value of the measured particle number concentrations (N) is shown in Fig. 8b. The scattering ($\sigma_{scat} = \alpha_{scat}/N$) and extinction ($\sigma_{ext} = \alpha_{ext}/N$) cross sections for each particle size were obtained by averaging the measurements of α_{scat} and α_{ext} at different concentrations. The scattering ($Q_{Scat} = 4\sigma_{Scat}/\pi D^2$) and extinction ($Q_{Ext} = 4\sigma_{Ext}/\pi D^2$) efficiencies were obtained as the ratio of the particle cross section to the geometric cross section. A plot of experimental Q_{scat} and Q_{Ext} as a function of particle diameter is shown in Fig. 8c. The retrieval algorithm of the RI was realized by fitting the measured scattering and extinction efficiencies to theoretically calculated values based on a Mie scattering subroutine, reported by Bohren and Huffman for homogeneous spheres (Bohren and Huffman, 1983; Laven, 2006). Best-fit results were obtained by varying the real and imaginary parts of the RI. A set of RI was found by minimizing the "merit function" $\chi^2\,\mathrm{Num}^{-2}$, where χ^2 is expressed as (Dinar et al., 2008; Zarzana et al., 2012; Washenfelder et al., 2013)

$$\chi^2(n,k) = \sum_{i=1}^{\mathrm{Num}} \frac{\left(Q_{\mathrm{scat,ext\_measured}} - Q_{\mathrm{scat,ext}}(n,k)\right)_i^2}{\Delta Q_i^2}, \qquad (6)$$

where Num is the number of measurements (of different particle sizes) used in the fit, $Q_{\mathrm{scat,ext}}\,(n,k)$ represents the scattering or extinction efficiencies, and ΔQ is the standard deviation of each measurement of the same particle size but at different concentrations.

The merit function was calculated for a wide range of n and k values, and the value of n and k that gives the lowest χ^2 (χ_0^2) was taken for the retrieved RI. The values of n and k that satisfy $\chi^2 < \chi_0^2 + 2.298$, which fall within the 1σ error bound of the best measurement (with 68.3 % confidence level of χ^2 distribution), are considered acceptable. Projections of the contour lines (with a contour value of 2.298) on the n and k plane give the standard errors Δn and Δk, respectively.

The RI of PSL was retrieved independently with scattering and extinction efficiencies, independently. The retrieved RI was $m = 1.676^{+0.009}_{-0.008} + i0.015^{+0.009}_{-0.008}$ from the scattering channel and $m = 1.674^{+0.012}_{-0.012} + i0^{+0.003}_{0}$ from the extinction channel. Limited by our aerosol generation system, the particles number concentrations were very small for the particle diameters larger than 400 nm. By using the efficiencies measured with small-particle diameters for the fit of the merit function, a non-zero value of the imaginary part of the RI could not be ruled out.

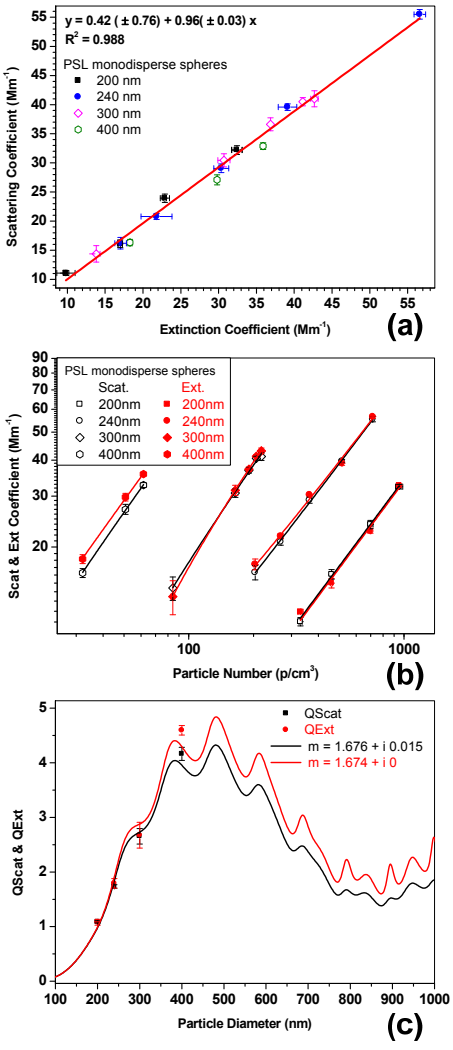

Figure 8. (a) Regression plot of the measured extinction and scattering coefficients, **(b)** scattering and extinction coefficients as a function of particle concentration, and **(c)** the scattering (Q_{Scat}) and extinction (Q_{Ext}) efficiencies as a function of particle diameter for monodisperse PSL spheres with four different particle diameters (200, 240, 300 and 400 nm) at $\lambda = 470$ nm.

Despite a number of previous studies previously performed, the differences between the retrieved RI values still span a range of about 5 % in the visible spectral region which is mainly due to the experimental difficulty in particulate measurements, in particular due to sample-to-sample differences depending on the nature of the preparation (Miles et al., 2010).

For PSL particles, Washenfelder et al. (2013) reported a RI value of $m = 1.633 + i0.005$ at $\lambda = 420$ nm. Chartier and Greenslade (2012) provided a value of $m = 1.72 + i0.005$ at $\lambda = 355$ nm; Abo Riziq et al. (2007), Lang-Yona et al. (2009) and Bluvshtein et al. (2012) (these studies are referred to as ALB hereafter) found a value of $m = 1.597 + i0.005$ at $\lambda = 532$ nm. Miles et al. (2010) published a value of $m = 1.627 + i0.0005$ at $\lambda = 560$ nm. Nikolov and Ivanov (2000) reported a value of $m = 1.617 + i0$ at $\lambda = 436$ nm and $m = 1.606 + i0$ at $\lambda = 486$ nm. Our results of $m = 1.676 + i0.015$ (retrieved from the scattering channel) and $m = 1.674 + i0$ (retrieved from the extinction channel) agree with the reported RI values as shown in Fig. 9. This result was a little larger than our previous result $m = 1.625 + i0.038$, which was probably caused by the large inner volume of the instrument and hence longer residual time (~ 200 s) and larger conglomeration effects on small-diameter particles. The larger particle loss leads to underestimation of the particle number concentration and overestimation of the extinction and scattering cross sections. Our results were in close agreement with the RI value give by Nikolov and Ivanov (2000) (interpolation of their data gave $m = 1.61 + i0$ at the wavelength of 470 nm). The difference between our retrieved refractive index and this interpolation value was about 4 %, within the tolerance of the instrumental accuracy (4 % for scattering and 5 % for extinction measurements, 3 % for particle concentration measurement), which confirmed that the calibration method used for determination of the cavity mirror reflectivity $R(\lambda)$, the scattering parameter K' and the parameter R_{L} (determined by calibration, too) was suitable for the aerosol optical-properties measurement.

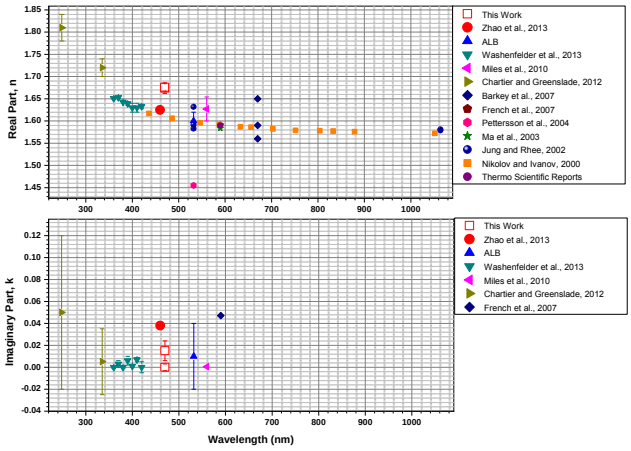

Figure 9. Survey of the measured values of real and imaginary part of refractive index versus wavelength for PSL.

3.5 Ambient measurement

For further evaluation and validation of the instrument developed, field environment measurements were carried out outside the laboratory at the Anhui Institute of Optics and Fine Mechanics (31°54′18″ N, 117°9′42″ E) during the period of 18–19 April 2013. Ambient air was sampled through a copper pipe (22 mm inner diameter) with an inlet about 5 m above the ground level. The acquisition time of the albedometer for each data was 9 s (for 1.5 s integrating time per spectrum, and six-spectra averaging). The cavity

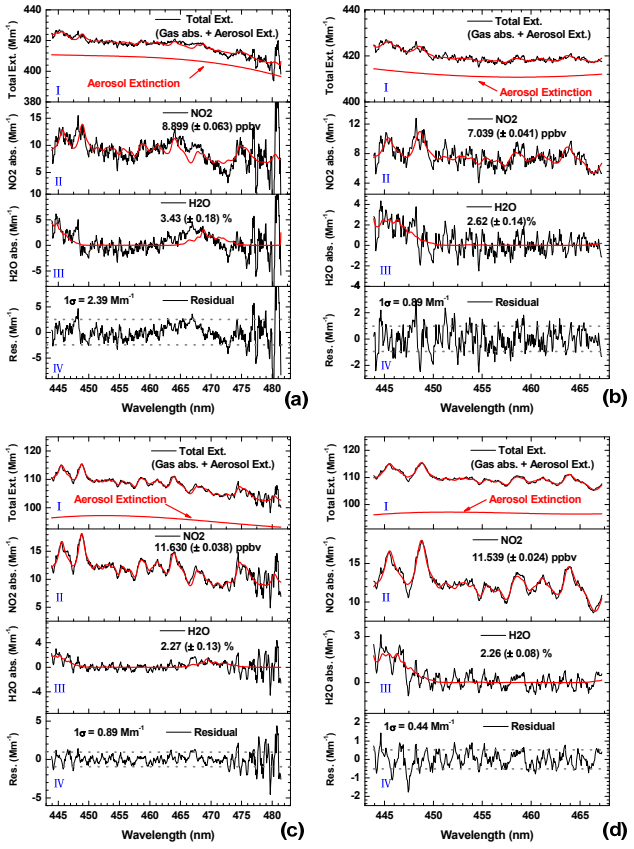

Figure 10. Example spectra from ambient measurements at different aerosol loadings. **(a)**, **(b)** Aerosol extinction larger than 400 Mm^{-1}; **(c)**, **(d)** aerosol extinction smaller than 100 Mm^{-1}. **(a)**, **(c)** Fit in a window of 444–481 nm for retrieval of aerosol extinction. **(b)**, **(d)** Fit in a window of 444–467 nm for NO_2 concentration retrieval. Black lines: measured spectra; red lines: aerosol extinction and reference spectra. (I): measured IBBCEAS spectra associated with the fitted spectra (including gas absorption and aerosol extinction). (II), (III): fitted NO_2 and H_2O absorption spectra. (IV) fit residuals.

was flushed with dry zero air every hour for acquisition of $I_0(\lambda)$ spectrum. The transmitted and scattered intensities of a particle-free (and non-absorbing) air sample were used to subtract the light scattered by internal surfaces and by gas portion of the sample.

An example of data retrieval is shown in Fig. 10 for ambient measurement at two different aerosol loadings: aerosol extinction larger than 400 Mm^{-1} (panels a, b) and lower than 100 Mm^{-1} (panels c, d) with different fit windows. A full window of 444–481 nm for aerosol extinction determination is shown in panels a and c, and a narrow window of 444–467 nm for NO_2 concentration retrieval is shown in panels b and d. The NO_2 cross section used reference was generated by convolution of high-resolution absorption cross sections reported by Vandaele et al. (2002), with the slit function of the spectrometer at 294 K. The H_2O absorption cross section was calculated based on the HITRAN 2008 database (HIgh-resolution TRANsmission molecular absorption database) (Rothman et al., 2009). The large fit error observed around 475–481 nm was due to the low signal-to-noise ratio (SNR) data related to low light transmission from the cavity. The detection sensitivity for ambient air measurements was lower than that obtained in particle-free sample measurement: approximately 6 times lower for the aerosols with extinction larger than 400 Mm^{-1} and 3 times lower for the extinction smaller than 100 Mm^{-1}. Under higher aerosol loading conditions (Fig. 10a), the detection sensitivity deteriorated. The big oscillation-like structure in the baseline at > 475 nm (due to the operation of the albedometer on the edge of the cavity bandwidth) and the absorption structure of aerosol around 465 to 470 nm interfered with the NO_2 concentration retrieved from the full window. The polynomial used in the DOAS fit did not completely account for the aerosol absorption feature. The absorption structure was not observed under lower aerosol loading conditions (Fig. 10c). Using an appropriate spectral region, good data retrieval is obtained (as shown in Fig. 10b).

An overview of ambient aerosol scattering, extinction coefficients, single-scattering albedo (SSA) and NO_2 concentration measured by the albedometer developed is shown in Fig. 11. The particle number concentration and the relative humidity are also shown in the upper panel. The relative humidity was measured using the internal relative humidity sensor of the TSI 3563 integrating nephelometer.

NO_2 concentrations retrieved from the IBBCEAS spectra were compared to the values measured with an online NO_x analyzer (Thermo 42i). Good agreement between two analytical instruments' measurements can be observed in Fig. 11 (middle panel), except for the period from 21:00 LT on 18 April to 06:00 LT on 19 April, where the results from the NO_x analyzer were about 1.2 ppbv larger than the albedometer measurements. This was probably caused by the interference of NO_y measured by the NO_x analyzer (equipped with a molybdenum converter) (Villena et al., 2012). However, these differences were still around the tolerance of the NO_x detection sensitivity (1 ppbv) for the used NO_x analyzer. An enlarged drawing of the NO_2 measurement comparison in two selected periods (10:00–15:00 LT on 18 April for high aerosol load conditions and 06:00–14:00 LT on 19 April for low aerosol loading) is shown in Fig. 12. NO_2 concentrations retrieved with different fit windows are also shown in the figure. An appropriate choice of the spectral region with good quality data was very important for accurate data retrieval (Fig. 10b, d). From a correlation plot of 5 min averaged data (Fig. 13), very good agreement was observed between the two instruments for different aerosol loadings (Albedometer = $0.995 \times NO_x$ analyzer + 0.465 ppbv, with $R^2 = 0.956$).

The aerosol scattering coefficient measured by the cavity-enhanced albedometer developed was compared with the data from an integrating nephelometer (TSI 3563) operating at three wavelengths centered at 453, 554 and 698 nm (the

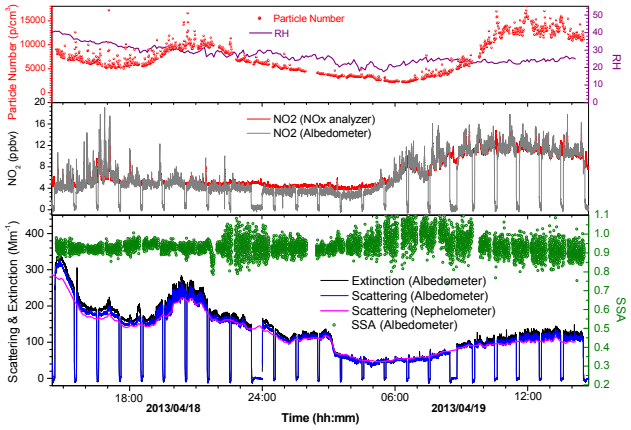

Figure 11. Ambient air measurements over 24 h using the cavity-enhanced albedometer developed. The acquisition time for each data point was 9 s. Upper panel: relative humidity of the air sample (purple line) measured with a humidity sensor, and particle concentration (red dot) measured with a CPC at the outlet. Middle panel: intercomparison of NO_2 concentration measurements (gray line) between the albedometer and a chemiluminescence detector (red line). Lower panel: aerosol scattering (blue line), extinction coefficients (black line) and the corresponding SSA (olive dots) determined at $\lambda = 470$ nm of the ambient air sample measured with the albedometer. The scattering coefficients are compared with the measurements from a TSI 3563 integrating nephelometer (magenta line). A good agreement between the albedometer and the TSI nephelometer is observed. The scattering coefficients measured with the cavity-enhanced albedometer are a little larger than that from the TSI 3563. This difference is probably due to the large-truncation-angle-induced scattering losses in the TSI nephelometer. The smaller truncation angle of our integrating sphere nephelometer allowed for collection of more scattered light.

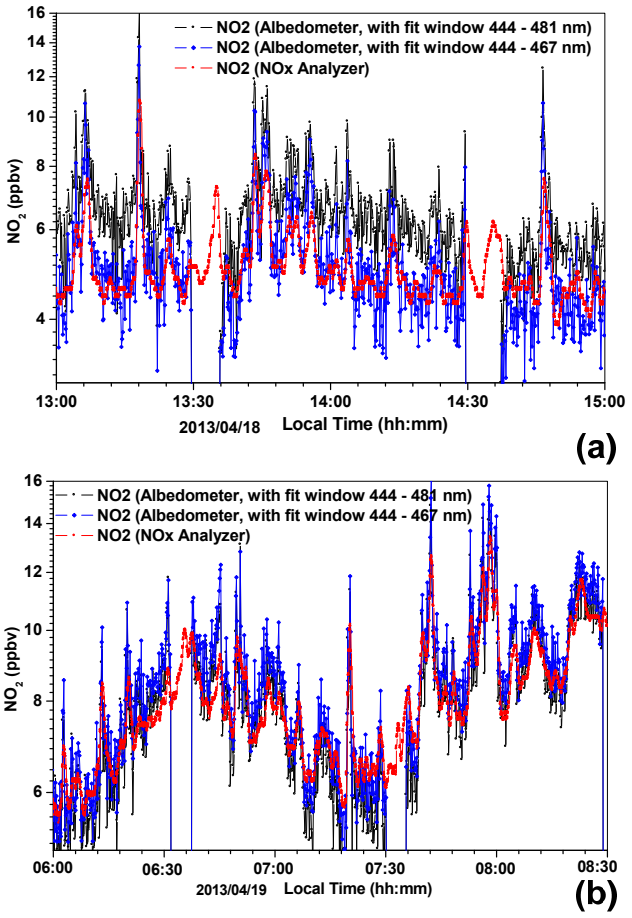

Figure 12. Comparison of NO_2 concentration measurements in representative time intervals between an NO_x analyzer (dotted red line) and the cavity-enhanced albedometer using different fit window (black: fitted over 444–481 nm, blue: fitted over 444–467 nm). **(a)** High aerosol extinction conditions and **(b)** low aerosol extinction conditions.

nominal values were 450, 550 and 700 nm, respectively) with a sampling flow of 20 L min^{-1}. The data averaging time was 300 s. Zero adjusting of the baseline for the scattering coefficient measurements was done automatically every hour. The scattering coefficient at 470 nm was calculated based on the value measured at 453 nm by the TSI 3563 nephelometer, using the following equation (Massoli et al., 2009; Huang et al., 2013):

$$\alpha_{\mathrm{scat},470} = \alpha_{\mathrm{scat},453}\left(\frac{470}{453}\right)^{-\text{å}}, \quad (7)$$

where the scattering Ångström exponent $\text{å} = -\frac{\log(\alpha_{\mathrm{scat},453}/\alpha_{\mathrm{scat},698})}{\log(453/698)}$ was calculated using the actual center wavelength values of 453 and 698 nm from the TSI 3563 nephelometer.

The scattering coefficients measured with the TSI 3563 agreed well with that from the albedometer, as shown in Fig. 11 (lower panel). An enlarged drawing of the scattering and extinction measurements in this time interval is shown in Fig. 14a. As can be observed, the albedometer's scattering measurements are larger than the values from the nephelometer when the extinction is large. This is due to the fact that under large extinction conditions, large-diameter particles dominated. The truncation error of the TSI 3563 nephelometer caused an underestimation of the scattering coefficient for the nephelometer. In the case of small extinction, fine particles are dominant and their loss due to conglomeration effects was larger in our system (as shown in Fig. 6), which leads to an underestimation of scattering and extinction coefficients for the albedometer. As shown in the figure, the albedometer's scattering values are consistently below the nephelometer's results. An appropriate choice of the flow rate could further minimize the particle loss (von der Weiden et al., 2009).

The correlation of the scattering coefficients measured with the two types of the instruments is plotted in Fig. 14b. Each data set was 5 min averaged. Scattering coefficient measurements with the albedometer are highly correlated with

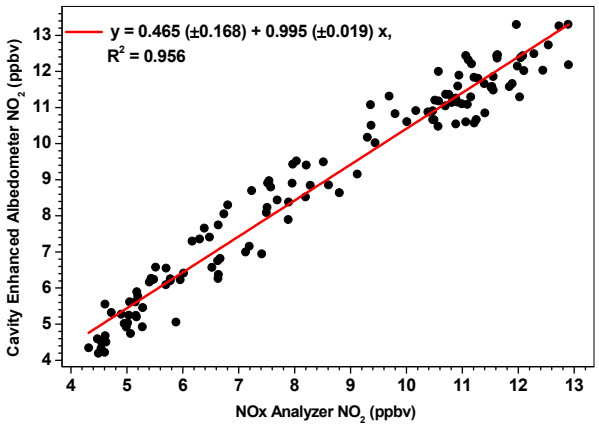

Figure 13. Correlation plots between NO_2 mixing ratios measured with the cavity-enhanced albedometer and an NO_x analyzer. All data were 5 min averaged.

those from the TSI 3563 (Albedometer = 1.13 × TSI Nephelometer − 9.44 Mm^{-1}, with $R^2 = 0.994$). The slope of 1.13 implicated that the smaller truncation angle of the integrating sphere used in the cavity-enhanced albedometer allowed for the collection of more scattered light compared to the TSI 3563 nephelometer. As shown in Fig. 3, for 1 µm diameter particles, the truncated fraction of total scattering was about 10 % with a truncation angle of 7°. And this value was increased to 20 % for particles of diameter of 1.5 µm. The intercomparison between the albedometer and the TSI nephelometer demonstrated the performance of our instrument for ambient air measurement.

4 Conclusions

The cavity-enhanced methods require very stable light sources. The LED is a promising new type of light source, with long lifetime and low energy consumption and it is more compact than commonly used broadband arc lamps (Ball et al., 2004). High-quality diode laser current and temperature controllers are usually used as LED controllers. In this way, high performance of the LED source (very stable emission spectrum and optical output power) is achievable with confidence, which allows high-sensitivity spectroscopic measurements of multi-species (aerosols and gases).

We report in this paper on the demonstration of an LED-based cavity-enhanced albedometer for simultaneous in situ measurement of aerosol scattering and extinction coefficients on the exact same sample volume. The performance of the instrument was evaluated using both laboratory-generated particles and ambient aerosols. The cavity-enhanced albedometer holds great promise for high-sensitivity and high-precision measurement of ambient aerosol scattering and extinction coefficients (hence SSA determination) and for absorbing trace gas concentration.

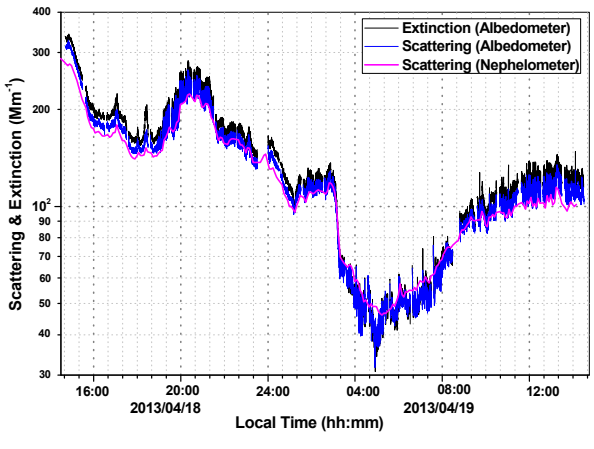

(a)

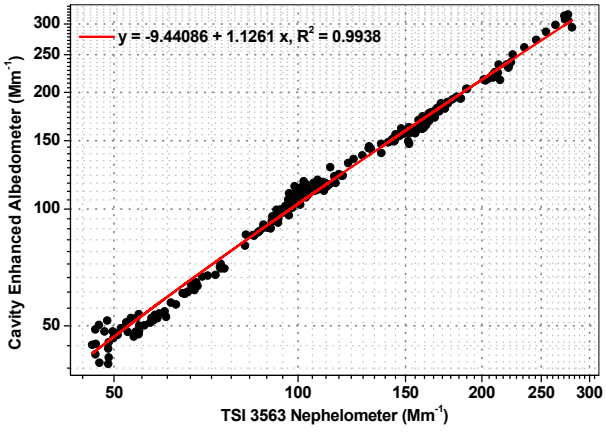

(b)

Figure 14. (a) Enlarged drawing of the scattering and extinction measurements of an air sample. The blue and black lines are the cavity-enhanced-albedometer-measured scattering and extinction coefficients, respectively. Magenta line is the scattering coefficient measured with a TSI integrating nephelometer. **(b)** Correlation plots of the scattering coefficients measured by the albedometer and a TSI 3563 nephelometer. All data were 5 min averaged.

The instrument's sensitivity and specificity demonstrated in the present work shows its potential for field observation on different platforms (ground observation networks, aircraft mapping, etc.), by benefiting from its capacity of distinguishing between aerosol extinction and trace gas absorption. In addition, simultaneous measurements of aerosol scattering and extinction coefficients enable a potential application for the retrieval of particle number size distribution and for faster retrieval of aerosols' complex RI. Moreover, unlike PAS technique, the measurement methods employed by the present albedometer are not (or much less) affected by RH, and hence well-suited to the measurements of aerosol optical properties at high RH, in particular for the determination of the complex RI of light-absorbing aerosols (such as black carbon and brown carbon) at high RH.

Currently, only one scattering coefficient can be measured due to the use of a single-channel PMT. When replacing this single-channel PMT with a multichannel PMT or a high-sensitivity spectrometer, measurement of broadband-wavelength-resolved scattering coefficients could be achievable. Employing a multi-cavity configuration could allow the albedometer to work in a wider wavelength range, from the UV to the near IR.

Acknowledgements. This research is supported by the Instrument Developing Project of the Chinese Academy of Sciences (YZ201121), the National Basic Research Program of China (2013CB955802), the National Natural Science Foundation of China (No. 41005017, 41330424, 41375127) and the China Special Fund for Meteorological Research in the Public Interest (GYHY201406039). The support of the CaPPA project ("Chemical and Physical Properties of the Atmosphere"), funded by the French National Research Agency through the "Programme d'Investissement d'Avenir" (under contract ANR-10-LABX-005), is acknowledged. We thank Liming Zhang, Zhengguo Shen and Xiuhong Qin in AIOFM for helpful discussions in the construction of the integrating sphere.

Edited by: M. Hamilton

References

Abo Riziq, A., Erlick, C., Dinar, E., and Rudich, Y.: Optical properties of absorbing and non-absorbing aerosols retrieved by cavity ring down (CRD) spectroscopy, Atmos. Chem. Phys., 7, 1523–1536, doi:10.5194/acp-7-1523-2007, 2007.

Abu-Rahmah, A., Arnott, W. P., and Moosmüller, H.: Integrating nephelometer with a low truncation angle and an extended calibration scheme, Meas. Sci. Technol., 17, 1723–1732, 2006.

Anderson, T. L. and Ogren, J. A.: Determining aerosol radiative properties using the TSI 3563 integrating nephelometer, Aerosol Sci. Tech., 29, 57–69, 1998.

Anderson, T. L., Covert, D. S., Marshall, S. F., Laucks, M. L., Charlson, R. J., Waggoner, A. P., Ogren, J. A., Caldow, R., Holm, R. L., Quant, F. R., Sem, G. J., Wiedensohler, A., Ahlquist, N. A., and Bates, T. S.: Performance characteristics of a high-sensitivity, threewavelength, total scatter/backscatter nephelometer, J. Atmos. Ocean. Technol., 13, 967–986, 1996.

Arnott, W. P., Moosmüller, H., Sheridan, P. J., Ogren, J. A., Raspet, R., Slaton, W. V., Hand, J. L., Kreidenweis, S. M., and Collett Jr., J. L.: Photoacoustic and filter-based ambient aerosol light absorption measurements: Instrument comparisons and the role of relative humidity, J. Geophys. Res., 108, 4034, doi:10.1029/2002JD002165, 2003.

Ball, S. M., Langridge, J. M., and Jones, R. L.: Broadband cavity enhanced absorption spectroscopy using light emitting diodes, Chem. Phys. Lett., 398, 68–74, 2004.

Barkey, B., Paulson, S. E., and Chung, A.: Genetic Algorithm Inversion of Dual Polarization Polar Nephelometer Data to Determine Aerosol Refractive Index, Aerosol Sci. Tech., 41, 751–760, 2007.

Baynard, T., Lovejoy, E. R., Pettersson, A., Brown, S. S., Lack, D., Osthoff, H., Massoli, P., Ciciora, S., Dube, W. P., and Ravishankara, A. R.: Design and application of a pulsed cavity ring-down aerosol extinction spectrometer for field measurements, Aerosol Sci. Tech., 41, 447–462, 2007.

Berden, G. and Engeln, R. (Eds.): Cavity Ring-Down Spectroscopy: Techniques and Applications, Wiley-Blackwell, 2009.

Bluvshtein, N., Flores, J. M., Abo Riziq, A., and Rudich, Y.: An approach for faster retrieval of aerosols' complex refractive index using cavity ring-down spectroscopy, Aerosol Sci. Tech., 46, 1140–1150, 2012.

Bohren, C. F. and Huffman, D. R.: Absorption and Scattering of Light by Small Particles, Wiley, New York, 1983.

Bond, T. C., Anderson, T. L., and Campbell, D.: Calibration and Intercomparison of Filter-Based Measurements of Visible Light Absorption by Aerosols, Aerosol Sci. Tech., 30, 582–600, 1999.

Boucher, O., Randall, D., Artaxo, P., Bretherton, C., Feingold, G., Forster, P., Kerminen, V.-M., Kondo, Y., Liao, H., Lohmann, U., Rasch, P., Satheesh, S. K., Sherwood, S., Stevens B., and Zhang, X. Y.: Clouds and Aerosols. In: Climate Change 2013: The Physical Science Basis. Contribution of Working Group I to the Fifth Assessment Report of the Intergovernmental Panel on Climate Change, Cambridge University Press, 2013.

Brown, S. S.: Absorption spectroscopy in high-finesse cavity for atmospheric studies, Chem. Rev., 103, 5219–5238, 2003.

Cappa, C. D., Lack, D. A., Burkholder, J. B., and Ravishankara, A. R.: Bias in filter-based aerosol light absorption measurements due to organic aerosol loading: evidence from laboratory Measurements, Aerosol Sci. Tech., 42, 1022–1032, 2008.

Chakrabarty, R. K., Moosmüller, H., Arnott, W. P., Garro, M. A., Slowik, J. G., Cross, E. S., Han, J. H., Davidovits, P., Onasch, T. B., and Worsnop, D. R.: Light scattering and absorption by fractal-like carbonaceous chain aggregates: comparison of theories and experiment, Appl. Optics, 46, 6990–7006, 2007.

Chakrabarty, R. K., Moosmüller, H., Chen, L.-W. A., Lewis, K., Arnott, W. P., Mazzoleni, C., Dubey, M. K., Wold, C. E., Hao, W. M., and Kreidenweis, S. M.: Brown carbon in tar balls from smoldering biomass combustion, Atmos. Chem. Phys., 10, 6363–6370, doi:10.5194/acp-10-6363-2010, 2010.

Chartier, R. T. and Greenslade, M. E.: Initial investigation of the wavelength dependence of optical properties measured with a new multi-pass Aerosol Extinction Differential Optical Absorption Spectrometer (AE-DOAS), Atmos. Meas. Tech., 5, 709–721, doi:10.5194/amt-5-709-2012, 2012.

Chin, M., Kahn, R. A., and Schwartz, S. E. (Eds.): Atmospheric Aerosol Properties and Climate Impacts, a Report by the US Climate Change Science Program and the Subcommittee on Global Change Research, National Aeronautics and Space Administration, Washington, DC, USA, 2009.

Cross, E. S., Onasch, T. B., Ahern, A., Wrobel, W., Slowik, J. G., Olfert, J., Lack, D. A., Massoli, P., Cappa, C. D., Schwarz, J. P., Spackman, J. R., Fahey, D. W., Sedlacek, A., Trimborn, A., Jayne, J. T., Freedman, A., Williams, L. R., Ng, N. L., Mazzoleni, C., Dubey, M., Brem, B., Kok, G., Subramanian, R., Freitag, S., Clarke, A., Thornhill, D., Marr, L. C., Kolb, C. E., Worsnop, D. R., and Davidovits, P.: Soot particle studies – instrument intercomparison – project overview, Aerosol Sci. Tech., 44, 592–611, 2010.

Dial, K. D., Hiemstra, S., and Thompson, J. E.: Simultaneous measurement of optical scattering and extinction on dispersed aerosol samples, Anal. Chem., 82, 7885–7896, 2010.

Dinar, E., Abo Riziq, A., Spindler, C., Erlick, C., Kiss, G., and Rudich, Y.: The complex refractive index of atmospheric and model humic-like substances (HULIS) retrieved by a cavity ring down aerosol spectrometer (CRD-AS), Faraday Discuss., 137, 279–295, 2008.

Dong, M., Zhao, W., Huang, M., Chen, W., Hu, C., Gu, X., Pei, S., Huang, W., and Zhang, W.: Near-ultraviolet incoherent broadband cavity enhanced absorption spectroscopy for OClO and CH_2O in Cl-initiated photooxidation experiment, Chinese J. Chem. Phys., 26, 133–139, 2013.

Dorn, H.-P., Apodaca, R. L., Ball, S. M., Brauers, T., Brown, S. S., Crowley, J. N., Dubé, W. P., Fuchs, H., Häseler, R., Heitmann, U., Jones, R. L., Kiendler-Scharr, A., Labazan, I., Langridge, J. M., Meinen, J., Mentel, T. F., Platt, U., Pöhler, D., Rohrer, F., Ruth, A. A., Schlosser, E., Schuster, G., Shillings, A. J. L., Simpson, W. R., Thieser, J., Tillmann, R., Varma, R., Venables, D. S., and Wahner, A.: Intercomparison of NO_3 radical detection instruments in the atmosphere simulation chamber SAPHIR, Atmos. Meas. Tech., 6, 1111–1140, doi:10.5194/amt-6-1111-2013, 2013.

Fiedler, S. E., Hese, A., and Ruth, A. A.: Incoherent broad-band cavity-enhanced absorption spectroscopy, Chem. Phys. Lett., 371, 284–294, 2003.

Fayt, C., De Smedt, I., Letocart, V., Merlaud, A., Pinardi, G., and Van Roozendael, M.: QDOAS Software user manual, available at: http://uv-vis.aeronomie.be/software/QDOAS/index.php (last access: 14 May 2012), 2011.

French, R. H., Winey, K. I., Yang, M. K., and Qiu, W. M.: Optical properties and van der Waals-London dispersion interactions of polystyrene determined by vacuum ultraviolet spectroscopy and spectroscopic ellipsometry, Aust. J. Chem., 60, 251–263, 2007.

Ghan, S. J. and Schwartz, S. E.: Aerosol properties and processes – a path from field and laboratory measurements to global climate models, B. Am. Meteorol. Soc., 88, 1059–1083, 2007.

Gherman, T., Venables, D. S., Vaughan, S., Orphal, J., and Ruth, A. A.: Incoherent broadband cavity-enhanced absorption spectroscopy in the near-Ultraviolet : application to HONO and NO_2, Environ. Sci. Technol., 42, 890–895, 2008.

Hallquist, M., Wenger, J. C., Baltensperger, U., Rudich, Y., Simpson, D., Claeys, M., Dommen, J., Donahue, N. M., George, C., Goldstein, A. H., Hamilton, J. F., Herrmann, H., Hoffmann, T., Iinuma, Y., Jang, M., Jenkin, M. E., Jimenez, J. L., Kiendler-Scharr, A., Maenhaut, W., McFiggans, G., Mentel, Th. F., Monod, A., Prévôt, A. S. H., Seinfeld, J. H., Surratt, J. D., Szmigielski, R., and Wildt, J.: The formation, properties and impact of secondary organic aerosol: current and emerging issues, Atmos. Chem. Phys., 9, 5155–5236, doi:10.5194/acp-9-5155-2009, 2009.

Huang, Y., Li, L., Li, J., Wang, X., Chen, H., Chen, J., Yang, X., Gross, D. S., Wang, H., Qiao, L., and Chen, C.: A case study of the highly time-resolved evolution of aerosol chemical and optical properties in urban Shanghai, China, Atmos. Chem. Phys., 13, 3931–3944, doi:10.5194/acp-13-3931-2013, 2013.

Jung, C. and Rhee, B. K.: Simultaneous determination of thickness and optical constants of polymer thin film by analyzing transmittance, Appl. Optics, 41, 3861–3865, 2002.

Kebabian, P. L., Robinson, W. A., and Freedman, A.: Optical extinction monitor using cw cavity enhanced detection, Rev. Sci. Instrum., 78, 063102, doi:10.1063/1.2744223, 2007.

Kennedy, O. J., Ouyang, B., Langridge, J. M., Daniels, M. J. S., Bauguitte, S., Freshwater, R., McLeod, M. W., Ironmonger, C., Sendall, J., Norris, O., Nightingale, R., Ball, S. M., and Jones, R. L.: An aircraft based three channel broadband cavity enhanced absorption spectrometer for simultaneous measurements of NO_3, N_2O_5 and NO_2, Atmos. Meas. Tech., 4, 1759–1776, doi:10.5194/amt-4-1759-2011, 2011.

Kraus, S. and Geyer, A.: DOASIS Jscript programming description, available at: http://www.iup.uni-heidelberg.de/bugtracker/projects/doasis (last access: 12 May 2012), 2001.

Lack, D. A., Lovejoy, E. R., Baynard, T., Pettersson, A., and Ravishankara, A. R.: Aerosol absorption measurement using photoacoustic spectroscopy: sensitivity, calibration, and uncertainty developments, Aerosol Sci. Tech., 40, 697–708, 2006.

Lack, D. A., Cappa, C. D., Covert, D. S., Baynard, T., Massoli, P., Sierau, B., Bates, T. S., Quinn, P. K., Lovejoy, E. R., and Ravishankara, A. R.: Bias in filter-based aerosol light absorption measurements due to organic aerosol loading: evidence from ambient measurements, Aerosol Sci. Tech., 42, 1033–1041, 2008.

Lack, D. A., Richardson, M. S., Law, D., Langridge, J. M., Cappa, C. D., McLaughlin, R. J., and Murphy, D. M.: Aircraft instrument for comprehensive characterization of aerosol optical properties, part 2: black and brown carbon absorption and absorption enhancement measured with photo acoustic spectroscopy, Aerosol Sci. Tech., 46, 555–568, 2012.

Lack, D. A., Moosmüller, H., McMeeking, G. R., Chakrabarty, R. K., and Baumgardner, D.: Characterizing elemental, equivalent black, and refractory black carbon aerosol particles: a review of techniques, their limitations and uncertainties, Anal. Bioanal. Chem., 406, 99–122, 2014.

Langridge, J. M., Richardson, M. S., Lack, D., Law, D., and Murphy, D. M.: Aircraft instrument for comprehensive characterization of aerosol optical properties, part I: wavelength-dependent optical extinction and its relative humidity dependence measured using cavity ringdown spectroscopy, Aerosol Sci. Tech., 45, 1305–1318, 2011.

Langridge, J. M., Richardson, M. S., Lack, D. L., Brock, C. A., and Murphy, D. M.: Limitations of the photoacoustic technique for aerosol absorption measurement at high relative humidity, Aerosol Sci. Tech., 47, 1163–1173, 2013.

Lang-Yona, N., Rudich, Y., Segre, E., Dinar, E., and Abo-Riziq, A.: Complex refractive indices of aerosols retrieved by continuous wave-cavity ring down aerosol spectrometer, Anal. Chem., 81, 1762–1769, 2009.

Laven, P.: MiePlot, available at: http://www.philiplaven.com/MiePlot.htm (last access: 2 July 2013), 2006.

Lewis, K., Arnott, W. P., Moosmüller, H., and Wold, C. E.: Strong spectral variation of biomass smoke light absorption and single scattering albedo observed with a novel dual wavelength photoacoustic instrument, J. Geophys. Res., 113, D16203, doi:10.1029/2007JD009699, 2008.

Li, L., Chen, J. M., Chen, H., Yang, X., Tang, Y., and Zhang, R.: Monitoring optical preperties of aerosols with cavity ring-down spectroscopy, J. Aerosol Sci., 42, 277–284, 2011.

Ma, L. and Thompson, J. E.: Optical properties of dispersed aerosols in the near ultraviolet (355 nm): measurement approach and initial data, Anal. Chem., 84, 5611–5617, 2012.

Ma, L., Cao, T., and Thompson, J. E.: Technical Note: Aeolian dust proxies produce visible luminescence upon intense

laser-illumination that results from incandescence of internally mixed carbon, Atmos. Meas. Tech. Discuss., 6, 5173–5194, doi:10.5194/amtd-6-5173-2013, 2013.

Ma, X. Y., Lu, J. Q., Brock, R. S., Jacobs, K. M., Yang, P., and Hu, X. H.: Determination of complex refractive index of polystyrene microspheres from 370 to 1610 nm, Phys. Med. Biol., 48, 4165–4172, 2003.

Massoli, P., Murphy, D. M., Lack, D. A., Baynard, T., Brock, C. A., and Lovejoy, E. R.: Uncertainty in light scattering measurements by TSI nephelometer: results from laboratory studies and implications for ambient measurements, Aerosol Sci. Tech., 43, 1064–1074, 2009.

Massoli, P., Kebabian, P. L., Onasch, T. B., Hills, F. B., and Freedman, A.: Aerosol light extinction measurements by Cavity Attenuated Phase Shift (CAPS) spectroscopy: laboratory validation and field deployment of a compact aerosol particle extinction monitor, Aerosol Sci. Tech., 44, 428–435, 2010.

Mellon, D., King, S. J., Kim, J., Reid, J. P., and Orr-Ewing, A. J.: Measurements of extinction by aerosol particles in the near-infrared using continuous wave cavity ring-down spectroscopy, J. Phys. Chem. A, 115, 774–783, 2011.

Michel Flores, J., Bar-Or, R. Z., Bluvshtein, N., Abo-Riziq, A., Kostinski, A., Borrmann, S., Koren, I., Koren, I., and Rudich, Y.: Absorbing aerosols at high relative humidity: linking hygroscopic growth to optical properties, Atmos. Chem. Phys., 12, 5511–5521, doi:10.5194/acp-12-5511-2012, 2012.

Miles, R. E. H., Rudic, S., Orr-Ewing, A. J., and Reid, J. P.: Influence of uncertainties in the diameter and refractive index of calibration polystyrene beads on the retrieval of aerosol optical properties using Cavity Ring Down Spectroscopy, J. Phys. Chem. A, 114, 7077–7084, 2010.

Moosmüller, H. and Arnott, W. P.: Angular truncation errors in integrating nephelometry, Rev. Sci. Instrum., 74, 3492–3501, 2003.

Moosmüller, H., Varma, R., and Arnott, W. P.: Cavity ring-down and cavity-enhanced detection techniques for the measurement of aerosol extinction, Aerosol Sci. Tech., 39, 30–39, 2005.

Moosmüller, H., Chakrabarty, R. K., and Arnott, W. P.: Aerosol light absorption and its measurement: a review, J. Quant. Spectrosc. Ra., 110, 844–878, 2009.

Müller, T., Nowak, A., Wiedensohler, A., Sheridan, P., Laborde, M., Covert, D. S., Marinoni, A., Imre, K., Henzing, B., Roger, J. C., dos Santos, S. M., Wilhelm, R., Wang, Y. Q., and de Leeuw, G.: Angular illumination and truncation of three different integrating nephelometers: implications for empirical, size-based corrections, Aerosol Sci. Tech., 43, 581–586, 2009.

Naus, H. and Ubachs, W.: Experimental verification of Rayleigh scattering cross sections, Opt. Lett., 25, 347–349, 2000.

Nikolov, I. D. and Ivanov, C. D.: Optical plastic refractive measurements in the visible and the near-infrared regions, Appl. Optics, 39, 2067–2070, 2000.

Pettersson, A., Lovejoy, E. R., Brock, C. A., Brown, S. S., and Ravishankara, A. R.: Measurement of aerosol optical extinction at 532 nm with pulsed cavity ring down spectroscopy, J. Aerosol Sci., 35, 995–1011, 2004.

Petzold, A., Onasch, T., Kebabian, P., and Freedman, A.: Intercomparison of a Cavity Attenuated Phase Shift-based extinction monitor (CAPS PMex) with an integrating nephelometer and a filter-based absorption monitor, Atmos. Meas. Tech., 6, 1141–1151, doi:10.5194/amt-6-1141-2013, 2013.

Platt, U. and Stutz, J.: Differential Optical absorption spectroscopy: principles and applications, Springer, 2008.

Platt, U., Meinen, J., Pöhler, D., and Leisner, T.: Broadband Cavity Enhanced Differential Optical Absorption Spectroscopy (CE-DOAS) – applicability and corrections, Atmos. Meas. Tech., 2, 713–723, doi:10.5194/amt-2-713-2009, 2009.

Ramanathan, V., Crutzen, P. J., Kiehl, J. T., and Rosenfeld, D.: Aerosols, climate, and the hydrological cycle, Science, 294, 2119–2124, 2001.

Rothman, L. S., Gordon, I. E., Barbe, A., Benner, D. C., Bernath, P. F., Birk, M., Boudon, V., Brown, L. R., Campargue, A., Champion, J.-P., Chance, K., Coudert, L. H., Dana, V., Devi, V. M., Fally, S., Flaud, J.-M., Gamache, R. R., Goldman, A., Jacquemart, D., Kleiner, I., Lacome, N., Lafferty, W. J., Mandin, J.-Y., Massie, S. T., Mikhailenko, S. N., Miller, C. E., Moazzen-Ahmadi, N., Naumenko, O. V., Nikitin, A. V., Orphal, J., Perevalov, V. I., Perrin, A., Predoi-Cross, A., Rinsland, C. P., Rotger, M., Šimecková, M., Smith, M. A. H., Sung, K., Tashkun, S. A., Tennyson, J., Toth, R. A., Vandaele, A. C., and Vander Auwera, J.: The HITRAN 2008 molecular spectroscopic database, J. Quant. Spectrosc. Ra., 110, 533–572, 2009.

Sanford, T. J., Murphy, D. M., Thomson, D. S., and Fox, R. W.: Albedo measurements and optical sizing of single aerosol particles, Aerosol Sci. Tech., 42, 958–969, 2008.

Sappey, A. D., Hill, E. S., Settersten, T., and Linne, M. A.: Fixed-frequency cavity ring down diagnostic for atmospheric particulate matter, Opt. Lett., 23, 954–956, 1998.

Schnaiter, M., Horvath, H., Möhler, O., Naumann, K. H., Saathoff, H., and Schöck, O. W.: UV-VIS-NIR spectral optical properties of soot and soot-containing aerosols, J. Aerosol Sci., 34, 1421–1444, 2003.

Shardanand, S. and Rao, A. D. P.: Absolute Rayleigh scattering cross sections of gases and freons of stratospheric interest in the visible and ultraviolet regions, NASA Technical Note, 1977.

Sharma, N., Arnold, I. J., Moosmüller, H., Arnott, W. P., and Mazzoleni, C.: Photoacoustic and nephelometric spectroscopy of aerosol optical properties with a supercontinuum light source, Atmos. Meas. Tech., 6, 3501–3513, doi:10.5194/amt-6-3501-2013, 2013.

Sheridan, P. J., Arnott, W. P., Ogren, J. A., Andrews, E., Atkinson, D. B., Covert, D. S., Moosmüller, H., Petzold, A., Schmid, B., Strawa, A. W., Varma, R., and Virkkula, A.: The Reno Aerosol Optics Study: an evaluation of aerosol absorption measurement methods, Aerosol Sci. Tech., 39, 1–16, 2005.

Slowik, J. G., Cross, E. S., Han, J. H., Davidovits, P., Onasch, T. B., Jayne, J. T., Williams, L. R., Canagaratna, M. R., Worsnop, D. R., Chakrabarty, R. K., Moosmüller, H., Arnott, W. P., Schwarz, J. P., Gao, R. S., Fahey, D. W., Kok, G. L., and Petzold, A.: An inter-comparison of instruments measuring black carbon content of soot particles, Aerosol Sci. Tech., 41, 295–314, 2007.

Smith, J. D. and Atkinson, D. B.: A portable pulsed cavity ring-down transmissometer for measurement of the optical extinction of the atmospheric aerosol, Analyst, 126, 1216–1220, 2001.

Sneep, M. and Ubachs, W.: Direct measurement of the Rayleigh scattering cross section in various gases, J. Quant. Spectrosc. Ra., 92, 293–310, 2005.

Stier, P., Seinfeld, J. H., Kinne, S., and Boucher, O.: Aerosol absorption and radiative forcing, Atmos. Chem. Phys., 7, 5237–5261, doi:10.5194/acp-7-5237-2007, 2007.

Strawa, A. W., Castaneda, R., Owano, T., Baer, D. S., and Paldus, B. A.: The measurement of aerosol optical properties using continuous wave cavity ring-down techniques, J. Atmos. Ocean. Technol., 20, 454–465, 2003.

Strawa, A. W., Elleman, R., Hallar, A. G., Covert, D., Ricci, K., Provencal, R., Owano, T. W., Jonsson, H. H., Schmid, B., Luu, A. P., Bokarius, K., and Andrews, E.: Comparison of in situ aerosol extinction and scattering coefficient measurements made during the aerosol intensive operating period, J. Geophys. Res., 111, D05S03, doi:10.1029/2005JD006056, 2006.

Subramanian, R., Roden, C. A., Boparai, P., and Bond, T. C.: Yellow beads and missing particles: trouble ahead for filter-based absorption measurements, Aerosol Sci. Tech., 41, 630–637, 2007.

Thalman, R. and Volkamer, R.: Inherent calibration of a blue LED-CE-DOAS instrument to measure iodine oxide, glyoxal, methyl glyoxal, nitrogen dioxide, water vapour and aerosol extinction in open cavity mode, Atmos. Meas. Tech., 3, 1797–1814, doi:10.5194/amt-3-1797-2010, 2010.

Thompson, J. E. and Spangler, H. D.: Tungsten source integrated cavity output spectroscopy for the determination of ambient atmospheric extinction coefficient, Appl. Optics, 45, 2465–2473, 2006.

Thompson, J. E., Smith, B. W., and Winefordner, J. D.: Monitoring atmospheric particulate matter through cavity ring-down spectroscopy, Anal. Chem., 74, 1962–1967, 2002.

Thompson, J. E., Barta, N., Policarpio, D., and DuVall, R.: A fixed frequency aerosol albedometer, Opt. Express, 16, 2191–2205, 2008.

Vandaele, A. C., Hermans, C., Fally, S., Carleer, M., Colin, R., Mérienne, M. F., Jenouvrier, A., and Coquart, B.: High resolution Fourier transform measurement of the NO_2 visible and near infrared absorption cross sections: temperature and pressure effects, J. Geophys. Res., 107, 4348, doi:10.1029/2001JD000971, 2002.

Varma, R., Moosmüller, H., and Arnott, W. P.: Toward an ideal integrating nephelometer, Opt. Lett., 28, 1007–1009, 2003.

Varma, R. M., Venables, D. S., Ruth, A. A., Heitmann, U., Schlosser, E., and Dixneuf, S.: Long optical cavities for open-path monitoring of atmospheric trace gases and aerosol extinction, Appl. Optics, 48, B159–B171, 2009.

Varma, R. M., Ball, S. M., Brauers, T., Dorn, H.-P., Heitmann, U., Jones, R. L., Platt, U., Pöhler, D., Ruth, A. A., Shillings, A. J. L., Thieser, J., Wahner, A., and Venables, D. S.: Light extinction by secondary organic aerosol: an intercomparison of three broadband cavity spectrometers, Atmos. Meas. Tech., 6, 3115–3130, doi:10.5194/amt-6-3115-2013, 2013.

Villena, G., Bejan, I., Kurtenbach, R., Wiesen, P., and Kleffmann, J.: Interferences of commercial NO_2 instruments in the urban atmosphere and in a smog chamber, Atmos. Meas. Tech., 5, 149–159, doi:10.5194/amt-5-149-2012, 2012.

Virkkula, A., Ahlquist, N., Covert, D., Sheridan, P., Arnott, W., and Ogren, J.: A three-wavelength optical extinction cell for measuring aerosol light extinction and its application to determining light absorption coefficient, Aerosol Sci. Tech., 39, 52–67, 2005.

von der Weiden, S.-L., Drewnick, F., and Borrmann, S.: Particle Loss Calculator – a new software tool for the assessment of the performance of aerosol inlet systems, Atmos. Meas. Tech., 2, 479–494, doi:10.5194/amt-2-479-2009, 2009.

Wang, L., Wang, W., and Ge, M.: Extinction efficiencies of mixed aerosols measured by aerosol cavity ring down spectrometry, Chinese Sci. Bull., 57, 2567–2573, 2012.

Washenfelder, R. A., Langford, A. O., Fuchs, H., and Brown, S. S.: Measurement of glyoxal using an incoherent broadband cavity enhanced absorption spectrometer, Atmos. Chem. Phys., 8, 7779–7793, doi:10.5194/acp-8-7779-2008, 2008.

Washenfelder, R. A., Flores, J. M., Brock, C. A., Brown, S. S., and Rudich, Y.: Broadband measurements of aerosol extinction in the ultraviolet spectral region, Atmos. Meas. Tech., 6, 861–877, doi:10.5194/amt-6-861-2013, 2013.

Wei, Y., Ma, L., Cao, T., Zhang, Q., Wu, J., Buseck, P. R., and Thompson, J. E.: Light scattering and extinction measurements combined with laser-induced incandescence for the real-time determination of soot mass absorption cross section, Anal. Chem., 85, 9181–9188, 2013a.

Wei, Y., Zhang, Q., and Thompson, J. E.: Atmospheric black carbon can exhibit enhanced light absorption at high relative humidity, Atmos. Chem. Phys. Discuss., 13, 29413–29445, doi:10.5194/acpd-13-29413-2013, 2013b.

Wilson, E. M., Chen, J., Varma, R. M., Wenger, J. C., and Venables, D. S.: A novel, broadband spectroscopic method to measure the extinction coefficient of aerosols in the near-ultraviolet, AIP Conf. Proc., 1531, 155–158, 2013.

Yu, F., Luo, G., and Ma, X.: Regional and global modeling of aerosol optical properties with a size, composition, and mixing state resolved particle microphysics model, Atmos. Chem. Phys., 12, 5719–5736, doi:10.5194/acp-12-5719-2012, 2012.

Zarzana, K. J., De Haan, D. O., Freedman, M. A., Hasenkopf, C. A., and Tolbert, M. A.: Optical Properties of the Products of α-Dicarbonyl and Amine Reactions in Simulated Cloud Droplets, Environ. Sci. Technol., 46, 4845–4851, 2012.

Zhang, R., Khalizov, A. F., Pagels, J., Zhang, D., Xue, H., and McMurry, P. H.: Variability in morphology, hygroscopicity, and optical properties of soot aerosols during atmospheric processing, P. Natl. Acad. Sci. USA, 105, 10291–10296, 2008.

Zhao, W., Dong, M., Chen, W., Gu, X., Hu, C., Gao, X., Huang, W., and Zhang, W.: Wavelength resolved optical extinction measurements of aerosols using broad-band cavity-enhanced absorption spectroscopy over the spectral range of 445–480 nm, Anal. Chem., 85, 2260–2268, 2013.